AMERICAN MUSEUM
Novitates

PUBLISHED BY THE AMERICAN MUSEUM OF NATURAL HISTORY
CENTRAL PARK WEST AT 79TH STREET, NEW YORK, NY 10024
Number 3474, 26 pp., 12 figures, 2 tables May 11, 2005

Age and Correlation of Fossiliferous Late Paleocene–Early Eocene Strata of the Erlian Basin, Inner Mongolia, China

GABRIEL J. BOWEN,[1] PAUL L. KOCH,[2] JIN MENG,[3] JIE YE,[4] AND SUYIN TING[5]

ABSTRACT

The Asian continent preserves a rich and diverse record of Paleogene mammal faunas and their evolution through time. The sequence of faunal succession is of key importance to our understanding of the origin and diversification of modern mammal groups, as phylogenetic data suggest that many major modern clades may be rooted in Asia. By calibrating the Asian fauna sequence within a chronostratigraphic framework, we can begin to compare patterns of succession on a global scale and constrain models for the origination and dispersal of modern mammal groups in the early Paleogene.

The Erlian Basin of Inner Mongolia preserves Early Paleogene strata and mammal fossils assignable to the Gashatan, Bumbanian, and Irdin Manhan Asian Land Mammal Ages (ALMAs). We measured stratigraphic sections and analyzed the stable isotope composition of paleosol carbonates and paleomagnetic directions of rocks at three localities in the Erlian Basin. The data document patterns in lithology, carbon isotope composition, and magnetic polarity that are consistent at all three localities and allow us to present two constrained hypotheses for the correlation of the local stratigraphic sections. Within the resulting composite section, we are able to identify a secular decrease in the carbon isotope composition of paleosol carbonate that can be equated to a multimillion-year trend preserved in late Paleocene and

[1] Current address: Department of Biology, University of Utah, Salt Lake City, UT, 84112 (gbowen@biology.utah.edu).
[2] Department of Earth Sciences, University of California, Santa Cruz, CA 95064 (pkoch@es.ucsc.edu).
[3] Division of Paleontology, American Museum of Natural History (jmeng@amnh.org).
[4] Institute of Vertebrate Paleontology and Paleoanthropology, Chinese Academy of Sciences, P.O. Box 643, Beijing 100044, P.R. China (jieye@yahoo.com).
[5] Museum of Natural Science, Louisiana State University, Baton Rouge, LA 70803 (glsuyin@lsu.edu).

 ISSN 0003-0082

early Eocene terrestrial and marine records. Using this trend and previously documented constraints on the age of the Bumbanian ALMA, the composite section is shown to correlate within the interval of time represented by chrons C26n–C24n of the Geomagnetic Polarity Timescale (GPTS). We outline three possible correlations of the sequence of magnetic polarity zones in our composite section to the GPTS and explore the biostratigraphic implications of these. All three possible correlations show that Gashatan faunas in Inner Mongolia occur within chron C24R, and the preferred correlation suggests that the Gashatan taxa may have persisted close to the Paleocene/Eocene boundary. If confirmed through further sampling, this result would imply that the first appearance of the modern mammal orders Primates, Artiodactyla, and Perissodactyla in Asia at the base of the Bumbanian ALMA did not significantly precede their first appearances in Europe and North America at the Paleocene/Eocene boundary. Fossil sites in the Erlian Basin promise to be central to resolving the debate about whether these clades lived and diversified in Asia before dispersing throughout the Northern Hemisphere at the Paleocene/Eocene boundary.

INTRODUCTION

The transition between the Paleocene and Eocene epochs was one of the most dynamic intervals of the Cenozoic. Long-term trends in climate ushered in the warmest period of the Cenozoic (Zachos et al., 2001). Throughout this gradual shift in climate, faunas and floras evolved in a series of abrupt events leading to the establishment of the first truly modern terrestrial ecosystems evidenced in the fossil record of the Holarctic continents. Abrupt changes in climate and faunal and floral composition coincided at the Paleocene/Eocene boundary, when transient global warming (e.g., Kennett and Stott, 1991), dispersal of mammal groups throughout the northern hemisphere (e.g., McKenna, 1973), and shifts in floral composition (Harrington, 2003) led to reorganization of terrestrial ecosystems on geologically short timescales (~100 thousand years (ky); Rohl et al., 2000; Bowen et al., 2001; Farley and Eltgroth, 2003).

One of the most profound changes in terrestrial ecosystems that occurred near the Paleocene/Eocene boundary was the abrupt first appearance of several modern groups of mammals in faunas from Asia, Europe, and North America (Gingerich, 1989; Hooker, 1998; Ting, 1998). The P/E first appearances included the first representatives of Primates, Artiodactyla, and Perissodactyla, three extant orders that went on to diversify and become important components of modern faunas, and Hyaenodontidae, a family of carnivorous mammals that suffered extinction in the Miocene (e.g., Gingerich, 1989). The abrupt appearance of these groups and lack of closely allied fossil outgroups in early Paleogene faunas led workers to conclude that the appearances represent immigration from an unseen locus of evolution (e.g., McKenna, 1973). Phylogenetic analysis of recently discovered Paleocene mammal fossils from China, however, has led some workers to conclude that Asian faunas include taxa closely allied to the new groups, and that the origins of the earliest Eocene debutants may be traced to a low-latitude Asian Eden (Beard, 1998; Beard and Dawson, 1999).

A simple test with the potential to verify Asia as a source of emigration at the Paleocene/Eocene boundary, if not as an evolutionary locus, would be to evaluate the relative age of the first appearances of clades on the three Holarctic continents. If the early representatives of one or more of the modern mammal groups were found to have greater antiquity in Asia than in Europe and North America, this would support Asia as a source of evolution or emigration. Conversely, finding that the Asian first appearances lagged or were synchronous with those on other continents would conflict with such a hypothesis.

Recent work has significantly clarified the relative age of early Paleogene faunal turnover events on the Holarctic continents. Of key importance is a globally correlatable carbon isotope excursion documented in marine and terrestrial sedimentary rocks (Koch et al., 1992; Zachos et al., 1993) and recently chosen as the defining stratigraphic datum for the Paleocene/Eocene boundary (Ouda, 2003). The base of the $\delta^{13}C$ excursion has been shown to correlate with the P/E first

appearances to within ~10 ky in North America (Bowen et al., 2001), where the new groups appear at the base of the Wasatchian North American Land Mammal Age (NALMA; Gingerich, 2001). Work in southern Europe has shown that the P/E first appearances there are unlikely to predate those in North America (Cojan et al., 2000). In northern Europe, taxa characteristic of the P/E first appearance event first appear at the Dormaal locality of Belgium (Smith, 2000). By correlation to other early Paleogene localities in Belgium and northern France for which bulk organic carbon isotope data are available, this fauna is thought to occur within the CIE and be time-equivalent to the earliest Wasatchian faunas (Steurbaut et al., 1999; Magioncalda et al., 2004).

In Asia, the first representative of Hyaenodontidae occurs in a fauna assigned to the Gashatan Asian Land Mammal age (ALMAs; Meng et al., 1998), which has been shown to be Late Paleocene in age (Bowen et al., 2002). Other important appearance events, however, including the first Asian primates, perissodactyls, and perhaps artiodactyls (Tong and Wang, 1998) occur within the subsequent Bumbanian ALMA (Dashzeveg, 1988; Ting, 1998). Earlier work (Bowen et al., 2002; Ting et al., 2003) has shown that the base of the Bumbanian is no younger than the P/E boundary, at ~55 million years ago (Ma; Wing et al., 1999), and that Gashatan index taxa persist at least until the end of chron C25n of the geomagnetic polarity timescale (GPTS) ~55.9 Ma (Cande and Kent, 1995). These correlations leave an unconstrained window of time some 900 ky long during which modern groups may have evolved and diversified in Asia or, alternatively, archaic groups may have persisted before the impending restructuring of their communities.

Here, our goal is to use magnetic and isotope stratigraphy to determine the age of mammal faunas from the Erlian Basin of Inner Mongolia (fig. 1). This region has produced several diverse collections of early Paleogene mammals, including several assemblages assigned to the Gashatan ALMA, and new fossiliferous levels and important specimens continue to be discovered (Meng et al., 2004; Smith et al., 2004). We present new lithological, biostratigraphic, paleomagnetic, and isotopic data from three fossil-bearing stratigraphic sections in the Erlian Basin. These data allow refined stratigraphic correlation of rock units within the basin and suggest correlations between these units and the GPTS. We then examine the implications of these correlations for the potential antiquity of the Bumbanian ALMA and associated modern mammal groups in Asia.

GEOLOGICAL SETTING

Fossil mammals of the Erlian Basin occur within a widely distributed package of siliciclastic sedimentary rocks. These rocks are largely undeformed and outcrop primarily in widely separated low mesas and in shallow washes. As a result of their poor local exposure and the relative isolation of outcrops in this region, stratigraphic correlation of rock units within the basin is difficult and no clear regional stratigraphy has been developed. Several stratigraphic units have been defined based on a combination of lithological and faunal characteristics, and these were recently reviewed by Meng et al. (1998, 2004).

The rocks at our study sites include red and tan mudstones, calcareous mudstones, and siltstones, commonly preserving millimeter-scale laminations of probable lacustrine origin, massive, brick red mudstone beds commonly preserving features indicative of paleosol development (see below), and laterally extensive sandstone and conglomerate beds of fluvial origin. These rocks have been previously assigned to the Nomogen, Arshanto, and Irdin Manha Formations, although the details of their assignment has differed among studies (see Meng et al., 2004). In many cases, these names refer to units recognized on the basis of combined lithostratigraphic and biostratigraphic characteristics, and as a result it is unclear how to assign many intervals in our local sections to these composite stratigraphic units. The stratigraphic nomenclature for the Erlian Basin is in need of revision, but because of the limited stratigraphic and geographic coverage of the present study we will not attempt such a revision here. Instead, we will refer throughout to informal lithostratigraphic

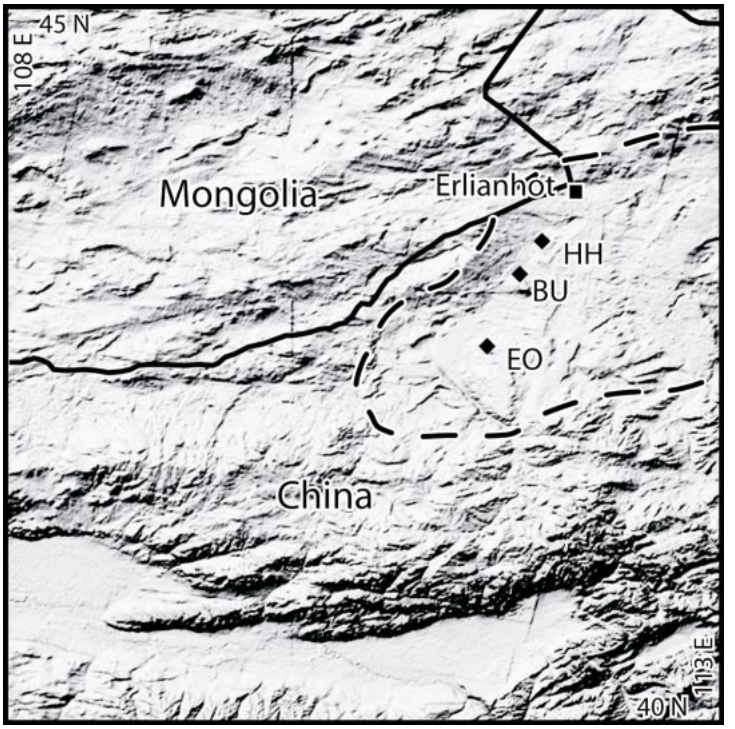

Fig. 1. Locality map for fossiliferous Early Paleogene sites in the Erlian Basin (dashed line), Inner Mongolia, China. Sites discussed in the text are Erden Obo (EO), Bayan Ulan (BU), and Huheboerhe (HH). All localities are to the southwest of the boarder town of Erlianhot (square). Digital relief from the GTOPO30 30′ × 30′ digital elevation model (U.S. Geological Survey, 1996).

units which we found to be useful in correlating among our local sections, with the intention that our findings might be incorporated into a comprehensive revision of the stratigraphy of the Erlian Basin in the future.

METHODS

We collected lithological data, fossils, oriented rock samples, and paleosol carbonate nodules from measured stratigraphic sections at three localities (figs. 1, 2). Sections were measured using a Jacob staff and described in the field from freshly exposed surfaces. Cores and blocks were collected for paleomagnetic analysis and oriented using a Brunton compass. Because exposure was poor, vertical horizination characteristic of soil development was not commonly observable in the field. Paleosols were identified as fine-grained siliciclastic rock units lacking internal stratification and containing features indicative of soil formation, including root traces, burrows, depletion channels, and carbonate nodules. Carbonate nodules were collected from paleosol beds on freshly exposed rock surfaces where there was no evidence of modern soil formation (e.g., modern roots, weathered textures).

Paleomagnetic analyses were conducted at the University of California paleomagnetics laboratory using a three-axis cryogenic superconducting magnetometer. Samples were incrementally demagnetized in a shielded oven at temperatures between 0 and 680°C. Directions were fit to the stepwise demagnetization data using least-squares analysis of vector component plots.

Samples of paleosol carbonate for stable carbon and oxygen isotope analysis were drilled from polished surfaces under magnification using a dental drill. Microcrystalline calcite was sampled exclusively; care was taken to avoid void-filling macrocrystalline phases which are likely to have formed dur-

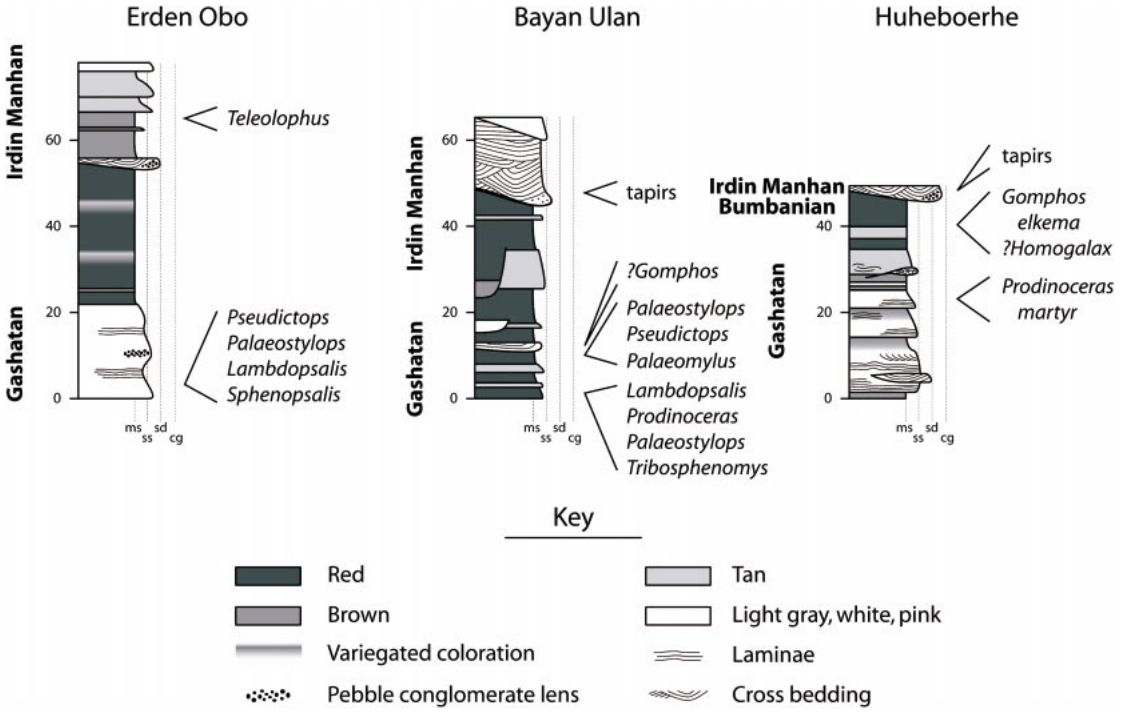

Fig. 2. Lithostratigraphic columns, key taxa, and faunal levels of the Erlian Basin sections. Biostratigraphic affiliation of taxa is shown to the left of each section.

ing post-burial diagenesis (e.g., Koch et al., 1995; Bao et al., 1998; Bowen et al., 2001). Samples were reacted with 100% H_3PO_4 in a common acid bath at 90°C, and the CO_2 evolved was cryogenically purified in an automated preparation device. The purified CO_2 was analyzed using a VG Optima or Prism gas source mass spectrometer, and sample values corrected relative to analyses of an in-house calcite standard. Isotope values are reported in per mil (‰) units and δ notation relative to the V-PDB standard, where $\delta = (R_{sample} - R_{standard})/R_{standard} * 1000$, and R indicates the ratio $^{13}C/^{12}C$ or $^{18}O/^{16}O$. Measurement precision was typically <0.05‰ for carbon and oxygen, based on repeated analyses of the calcite standard.

RESULTS

Lithostratigraphy and Faunal Levels

At Erden Obo (42°73′N, 111°21′E), the basal ~21 m of the section consist of medium to coarse-grained sandstone, soft, pink, laminated siltstone, and lenses of pebble conglomerate. Fragmentary fossil vertebrate remains, including specimens of the anagalid *Pseudictops*, arctostylopid *Palaeostylops*, and multituberculates *Lambdopsalis* and *Sphenopsalis*, occur in the lower ~5 m of the section (fig. 2). At the 21-m level there is a transition to fine-grained rocks, and from 21 to 55 m there is a series of variegated red-brown to gray-green unfossiliferous mudrocks. These are capped by a thin (~0.5 m) medium-coarse-grained sandstone with a sharp, undulatory basal contact. The sandstone contains quartz pebbles lenses and abundant fragmentary vertebrate fossils. Between 55.5 m and the top of the section reported here (78 m) is a series of interbedded brown and tan siltstones and fine- to medium-grained sandstones. These are typically <3.5 m thick, and produce fossils at several levels, including the tapiroid perissodactyl *Teleolophus* at ~65 m.

The sampled section at Bayan Ulan (43°08′N, 111°35′E), some 40 km NNE of Erden Obo (fig. 1), consists primarily of nonbedded red, tan, and brown siltstones and

Fig. 3. Field photograph of mud-filled channels at Bayan Ulan. The patchily distributed light-colored rock in the foreground of the photo is soft, white, silty mudstone containing pockets of rounded clayball conglomerate, which fills a sinuous channel incised into the surrounding hard, orange-red mudrock. The top of this channel could not be located in the field area. An upper channel, ~5 m deep, can be seen on the ridge (black arrows). This feature cuts perpendicular to the plane of the photograph and is filled with white mudstone. A geologist is standing at the left of the photo (white arrow) in a plane between the two channels, providing an approximate indication of the scale of these features.

mudstones. Within the lower 48 m of the measured section, red-brown mudstone beds up to 7.5 m thick are dominant and are interbedded with thinner, white, tan and brown siltstone beds (fig. 2). Near the base of the section these beds are fossiliferous, and the Bayan Ulan fauna of Meng et al. (1998) was collected from the basal ~3 m of our section. The dominant taxon at this level is the multituberculate *Lambdopsalis*. Other ''index'' fossils from this level include *Palaeostylops*, the dinoceratid *Prodinoceras*, and *Tribosphenomys* (a gliroid). During our fieldwork of 2002, we found a fossiliferous level at 8–9 m of the section (BU-01-01-04 was taken at 8 m; this is the fossil site 02–02), from which numerous specimens of small mammals including *Palaeostylops*, *Pseudictops*, and a new basal gliroid (Meng et al., 2005) were collected. There is no specimen of *Lambdopsalis* from this level, and this fossil assemblage may represent a slightly younger fauna than the previously described Bayan Ulan fauna (Meng et al., 2005). Slightly above this level, two calcanea that are similar to those of *Gomphos* were found (Meng et al., 2004). The main lithologic transition in the Bayan Ulan section occurs at the 48 m level, where nonbedded red mudstones are erosionally truncated by a stacked complex of crossbedded to laminated, gray-white siltstone and fine-grained sandstone. Tapiroid fossils were collected from a bed just below this transition.

Within the mudstone interval comprising the basal 48 m of the Bayan Ulan section we observed several scours and fine-grained sand or mud-filled channels (figs. 2, 3). These appear to cut several meters into the underlying strata, and add considerable stratigraphic complexity to the section, and in some cases these beds may produce mammal fossils that, without careful consideration for their stratigraphic context, might lead to erroneous interpretation of the biostratigraphy of the section. We found it to be necessary to run our measured section through one mud-filled channel, and took note of its position. Although section meter levels reported for Bayan Ulan do not take into account the depth of this erosional surface, they do reflect the proper superpositional order of the sites considering their stratigraphic context.

Our third section was measured at Huheboerhe (43°22′N, 111°45′E), and is a revised

version of the section of Meng et al. (2004) reflecting new observations made during the 2004 field season. At Huheboerhe, the basal 24 m of section consist of lens-shaped, cross-bedded, fine- to medium-grained sandstones, soft, pink, laminated sandy siltstones, and brechiated to homogeneous, red-weathering mudstones. Within this package, finer grained rock types become increasingly dominant up-section. The uppermost sandy siltstone bed produced a specimen of *Prodinoceras* (23 m). The interval between 24 and 47.5 m is predominately mudstone. Beds near the base of this interval are tan and brown, with a transition to gray mudstone and a single, thick (7.5 m) red mudstone occurring at the 40-m level. Specimens of the basal gliroid *Gomphos elkema* (Meng et al., 2004), a small perissodactyl, possibly *Homogalax*, and a hyaenodontid smaller than *Prolimnocyon chowi* (Meng et al., 1998) were recovered from this red bed during fieldwork in 2002; very large (up to 10 cm diameter) paleosol carbonate nodules were also found near the base of the bed. Screen-washing sediments from this bed in 2004 yielded teeth of at least two species of small rodents. These rodents are generally similar to those from the Bumban beds of Mongolia (Shevyreva, 1989; Dashzeveg, 1990). However, because the rodent specimens from the Bumban beds are fragmentary and their taxonomic identifications are currently uncertain (Averianov, 1996), we do not provide preliminary identifications of the Huheboerhe specimens in this study to avoid further complication of the situation.

Lower in the mudstone interval, at 28.5 m, pods of hard, brittle, carbonate grainstone up to ~50 cm in diameter were observed weathering out in a discrete horizon. These are comprised primarily of round, carbonate-coated clayballs several millimeters in diameter, and are tentatively interpreted as fossil cold spring deposits. At the top of the section, a coarse-grained sandstone and pebble conglomerate overlies the thick red mudstone with a sharp basal contact. The conglomerate contains abundant fragmentary vertebrate fossils, including tapiroid perissodactyls. Fragmentary fossils from the conglomerate bed have washed down and can be found on the surface of the underlying, uppermost red mudstones. Particular care must be taken in interpreting the provenance of fossils collected from these mudstone beds.

The biostratigraphic affiliations of many index taxa from the Erlian Basin sections are shown in figure 2. *Prodinoceras*, *Palaeostylops*, *Tribosphenomys*, and the multituberculates are all indicative of the Gashatan ALMA, and most of the collections from the Erlian Basin sections that bear these taxa represent assemblages that are compositionally similar to other assemblages of Gashatan age (Ting, 1998). The only taxon in our sections that is considered diagnostic of the Bumbanian ALMA is *G. elkema* (Dashzeveg, 1988; Meng et al., 2004). Fossil tapirs are characteristic of subsequent ALMAs, which have been termed the Arshantan and Irdin Manhan. These biostratigraphic units are weakly defined based on a combination of lithological and faunal associations, and are in need of review. Because the tapir specimens and associated fossils referred to here were collected from strata overlying the Bumbanian and Gashatan levels that have been described as the ''Irdin Manha beds'', we will describe them as representing the Irdin Manhan ALMA.

PALEOMAGNETICS

Samples from the Erlian Basin sections ($N = 183$) displayed a wide array of magnetic behaviors during stepwise demagnetization, but many siltstone samples and some mudstones exhibited relatively stable behavior. Demagnetization of these samples typically revealed multiple directional components (fig. 4). Most samples preserved a low-temperature component, which was removed at temperatures below 300°C and exhibits an average declination (D) of 355° and inclination (I) of 75° ($N = 177$; fig. 5A). We interpret this component to be a modern field overprint. Stable samples also typically preserved a second, characteristic direction, which was removed between 300 and 580°C (fig. 4). This component exhibits directions indicative of both normal and reversed fields, and the average directions for normal and reversed field samples are roughly antipodal ($D = 10.6°$, $I = 48.0°$, $N = 84$, $k = 5.614$, and $D = 191.5°$, $I = -42.7°$, $N = 58$, $k = 6.215$,

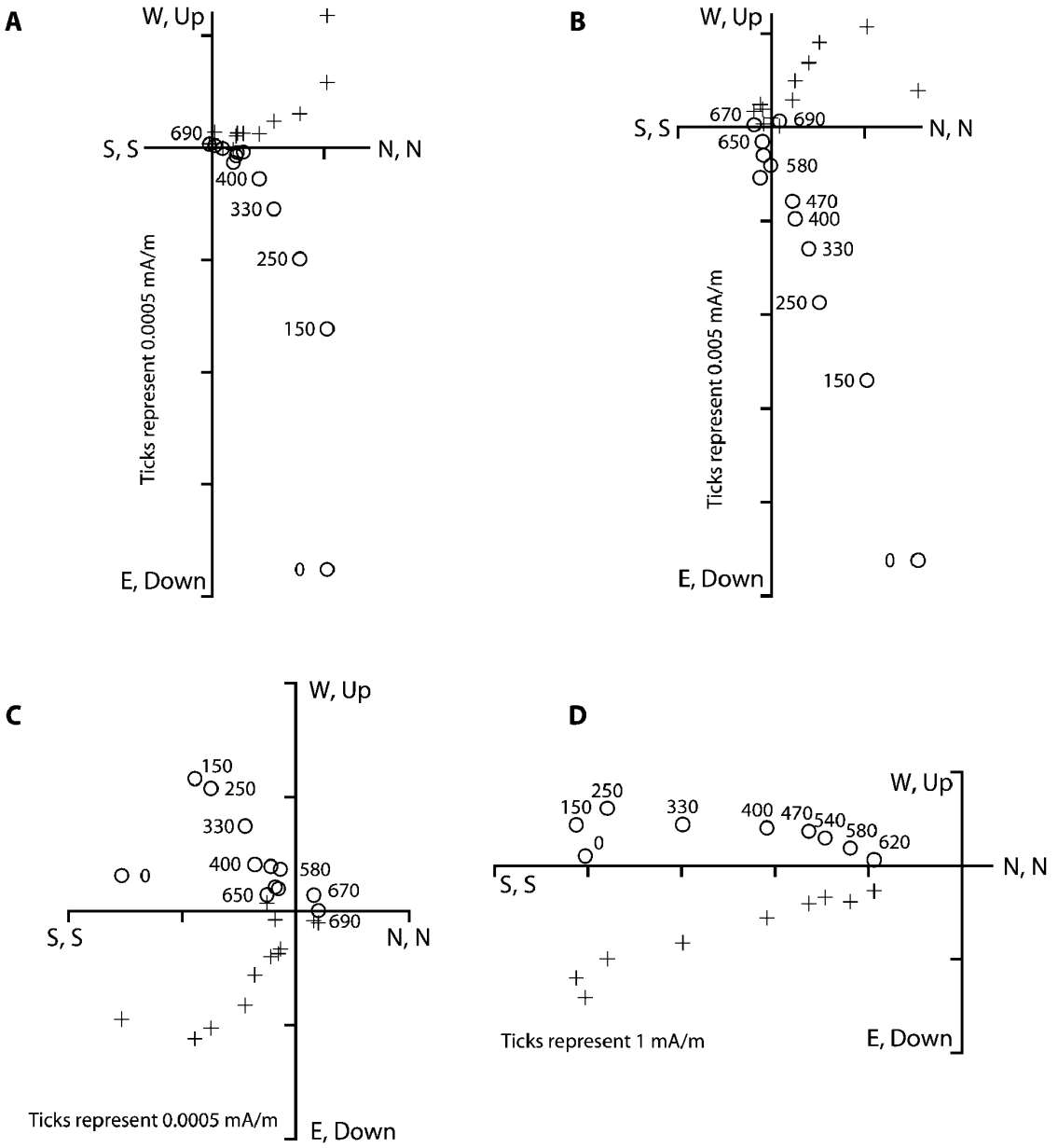

Fig. 4. Vector component diagrams for the thermal demagnetization of Erlian Basin samples. Crosses show the horizontal magnetization component and circles the vertical component projected on the N–S vertical plane. Labels indicate the thermal temperature step (°C) for each vertical plane point. Note the relatively stable demagnetization behavior of samples with a wide range of remanence intensities. **A,** BU020109A and **B,** BU020111C, samples characterized by normal field directions. **C,** BU020101C and **D,** HH020101E, samples preserving reversed field directions. All samples depicted here show the removal of a normal field overprint at temperatures <300°C and isolation of a characteristic component between 300 and 580°C.

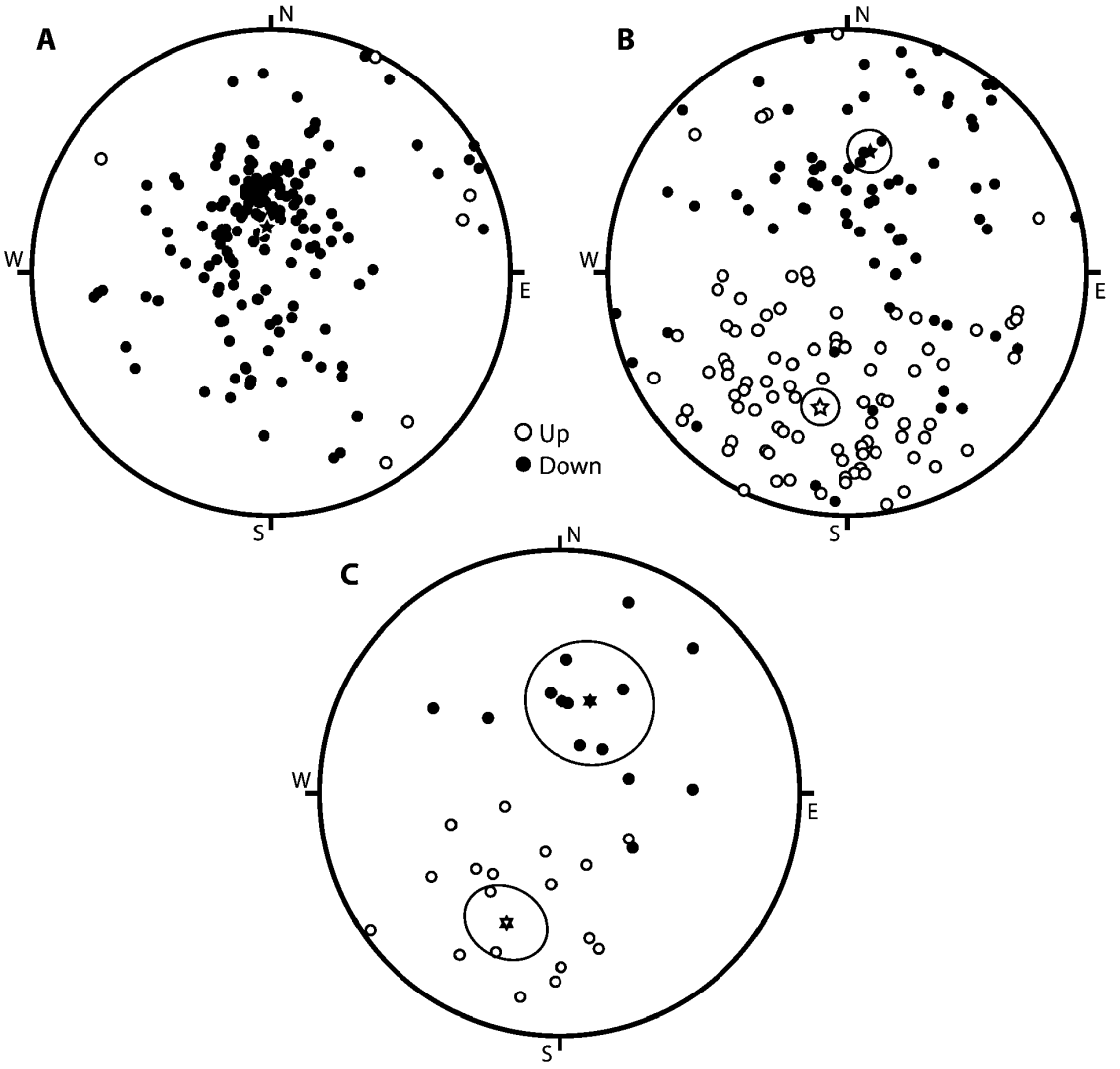

Fig. 5. Equal-area projections of sample and site mean remanence directions. Mean directions for each polarity are shown with stars, and circles represent α95. **A,** Low temperature component, isolated below 300°C, for individual samples. The mean direction of this component ($D = -5°$, $I = 75°$) is similar to the expected modern-field direction for the Erlian Basin ($D = 0°$, $I = 62°$), with the somewhat steeper inclination likely reflecting the partial removal of primary reversed polarity magnetization from some samples at low temperature. **B,** Characteristic component, isolated between 300 and 580° C. **C,** Site mean directions, calculated from sample characteristic component directions. Mean normal and reversed site directions are similar to previously reported directions from the Tertiary of Inner Mongolia (Zhao et al., 1994).

respectively; fig. 5B). The unblocking temperature of this component suggests that it was carried by magnetite, and we interpret it to be depositional remanent magnetization carried by detrital magnetite grains.

Site average directions were calculated for sites with multiple stable samples (table 1). These were classed as alpha or beta sites according to data quality, with alpha sites having four or more samples clustered at 99% confidence and beta sites having two sites clustered at 99% confidence or three or more

TABLE 1
Paleomagnetic Data

Site[a]	Level (m)	D site[b]	I site[b]	α95	*N*	*R*	*k*
			Erden Obo				
EO-01–27	67.5	12.1	−61.8		1	1.00	
EO-01-25	*62*	*2.8*	*44.2*	*40.2*	*3*	*2.81*	*10.46*
EO-01-23	57.5	44.8	69.4		1	1.00	
EO-01-22	54.8	78.8	66		1	1.00	
EO-01-18	**43**	**88.6**	**44**	**28.6**	**4**	**3.73**	**11.30**
EO-01-15	*36.5*	*253.9*	*−51.2*	*46.9*	*2*	*1.97*	*30.52*
EO-01-07	**24.5**	**237**	**−36.6**	**11**	**5**	**4.92**	**49.57**
EO-01-05	**23.9**	**215.3**	**−48.7**	**15.1**	**4**	**3.92**	**37.93**
EO-01-04	17.2	193.8	−69.7	180	2	1.68	3.13
EO-01-02	**13.5**	**32**	**48.5**	**23.4**	**4**	**3.82**	**16.33**
EO-01-01	9	354.8	56.1	117	3	2.11	2.26
			Bayan Ulan				
BU-02-01-13	**48**	**20.2**	**17.8**	**16.2**	**5**	**4.83**	**23.33**
BU-02-01-11	**46.5**	**315.7**	**54.8**	**10.3**	**5**	**4.93**	**55.86**
BU-02-01-10	**46**	**126.6**	**58.8**	**41.9**	**4**	**3.48**	**5.77**
BU-02-01-09	*44*	*303.4*	*37.2*	*43.3*	*3*	*2.78*	*9.19*
BU-02-02-01	**42.5**	**1.3**	**59.1**	**8.3**	**5**	**4.95**	**86.97**
BU-02-01-08	**39.5**	**5.5**	**59.7**	**23.4**	**5**	4.66	**11.68**
BU-02-01-07	**34.5**	**23.5**	**72.6**	**16.7**	**5**	4.82	**21.90**
BU-02-01-03	**27**	**165.7**	**−34.3**	**19.9**	**4**	3.87	**22.29**
BU-02-01-04	25	179.6	−29.1	180	2	1.77	4.32
BU-02-01-02	**22**	**185.4**	**−58.9**	**31.1**	**4**	**3.69**	**9.72**
BU-02-01-01	**15**	**195.3**	**−64**	**17.6**	**5**	**4.80**	**19.83**
BU-01-01-06	*13*	*228*	*−51.2*	*48*	*2*	*1.97*	*29.17*
BU-01-01-04	**8**	**234.5**	**−3.3**	**13.4**	**5**	**4.88**	**33.62**
BU-01-01-03	*5*	*256.1*	*−70.8*	*12.3*	*3*	*2.98*	*101.63*
BU-01-01-02	**3.2**	**219.8**	**−54.1**	**33.9**	**5**	**4.34**	**6.06**
BU-01-01-01	**1.5**	**168.2**	**−39**	**8.8**	**4**	**3.97**	**111.08**
			Huheboerhe				
HH-02-01-10	*53.8*	*191.1*	*−15.4*	*40.4*	*3*	*2.81*	*10.36*
HH-02-01-08	**44.8**	**212**	**−22.6**	**18.4**	**4**	**3.88**	**25.94**
HH-02-01-05	**40.3**	**181.4**	**−23.4**	**21.9**	**5**	**4.70**	**13.17**
HH-02-01-04	**36.8**	**42.9**	**19.7**	**18.4**	**5**	**4.78**	**18.28**
HH-02-01-03	**35.3**	**202.1**	**−30.1**	**26.7**	**4**	**3.77**	**12.82**
HH-02-01-02	**32.2**	**200.3**	**−28.1**	**19.1**	**5**	**4.76**	**17.01**
HH-02-01-01	**30.3**	**167.2**	**−18.6**	**13.3**	**5**	**4.88**	**34.04**

[a] Sites are classed as alpha (bold), beta (italics), or poorly clustered (normal font) according to data quality as described in the text.

[b] Site average declination (D) and inclination (I).

sites clustered at 95% confidence, according Watson's test for randomness (Watson, 1956). Site mean directions for normal and reversed sites are roughly antipodal (D = 18.8°, I = 57.3°, N = 11, k = 5.551, and D = 202.4°, I = −41.7°, N = 17, k = 8.108, respectively; fig. 5C). When plotted stratigraphically, the site average directions define coherent polarity intervals in all three sections (fig. 6). At Erden Obo, two polarity transitions are preserved. A basal normal polarity zone is indicated by data from a single alpha site, but supported by data from two other sites with poor clustering that suggest this zone encompasses at least the 9- to 16.5-m levels of our section. Sites from the middle

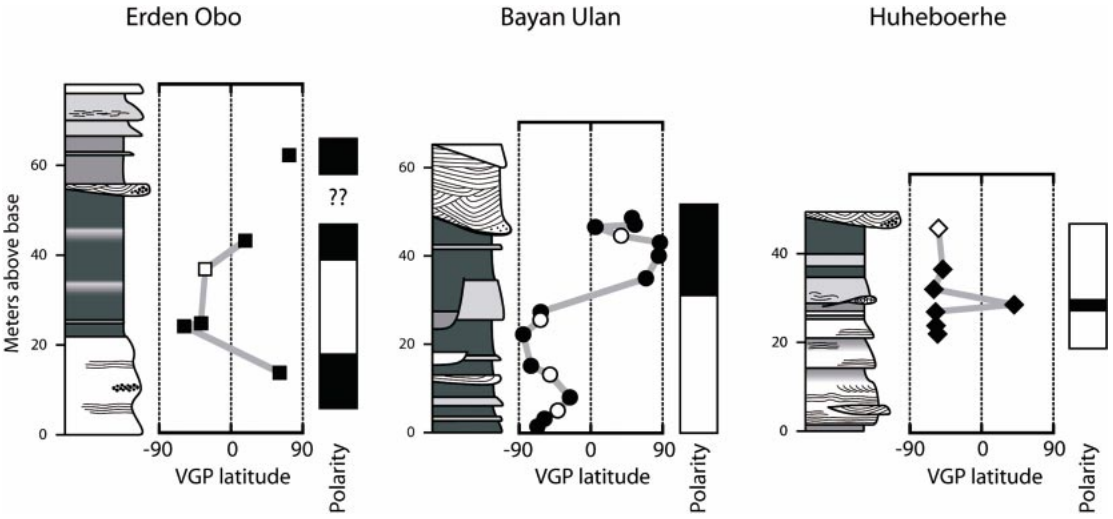

Fig. 6. Virtual geomagnetic pole (VGP) latitudes calculated from site mean directions and interpreted pattern of polarity reversals for the three study sections. VGP data are classed by data quality, as described in the text; here, closed symbols represent alpha sites and open symbols represent beta sites. Lithostratigraphic symbols as in figure 2.

~20 m of the section demonstrate reversed polarity, and those above the 40 m level are characterized by normal polarity. The Bayan Ulan section contains two relatively well-defined polarity zones, with a transition from reversed to normal polarity occurring between 27 and 34.5 m. Our sampling at this site shifts into a ~10 m deep, mud-filled channel between 25 and 27 m, and an unknown amount of time is represented by erosional surface at the base of this channel. Site BU-02-01-03, within the lowermost channel-filling beds, preserves a reversed direction similar to that of the adjacent site BU-02-01-04, which lies outside the channel. The most parsimonious interpretation of this observation is that the time represented by the erosional surface occurred within a single interval of reversed polarity. With the exception of one alpha site at 28.5 m, all sampled sites at Huheboerhe preserve well-constrained, reversed field directions.

Stable Isotopes

Analyses of the $\delta^{13}C$ and $\delta^{18}O$ values of 73 carbonate nodules from 30 sampling levels are shown in table 2 and figure 7. The average range for multiple $\delta^{13}C$ or $\delta^{18}O$ analyses from a single nodule is 0.15 and 0.17‰ (N = 63), and for multiple nodules from a single sampling level is 0.94 and 0.93‰ (N = 29), respectively. No pervasive pattern of covariation between carbon and oxygen isotopes is observed in the raw data set (fig. 7A), but covariation is observed between the mean $\delta^{13}C$ and $\delta^{18}O$ values of nodules from single sampling levels (fig. 7B). When site mean $\delta^{13}C$ values are plotted against stratigraphic level, all three localities show up-section decreases in $\delta^{13}C$ (fig. 8). The trend is particularly well defined within the Bayan Ulan section. At Erden Obo, there is an ~35-m sampling gap in the middle of the section, but samples near the top of the section have $\delta^{13}C$ values 2–3‰ lighter than those at ~20 m. Samples from Huheboerhe have relatively variable $\delta^{13}C$ values, but level averages suggest that the sampled interval may be characterized by a weak decrease in $\delta^{13}C$ up-section.

DISCUSSION

Fidelity of the Paleomagnetic Record

Several lines of evidence suggest that characteristic directions isolated in Erlian Basin paleomagnetic samples preserve information about the magnetic field at the time

TABLE 2
Stable Isotope Data

Nodule	Sample	Level (m)	Sample		Nodule		Level	
			$\delta^{13}C$	$\delta^{18}O$	$\delta^{13}C$	$\delta^{18}O$	$\delta^{13}C$	$\delta^{18}O$
				Erden Obo				
EO-01-27+0.5-1	A	68.0	−6.84	−10.48	−6.86	−10.41	−7.01	−10.65
	B		−6.89	−10.33				
EO-01-27+0.5-2	A		−7.10	−10.85	−7.15	−10.89		
	B		−7.21	−10.92				
EO-01-26+0.5-1	A	64.5	−7.48	−9.07	−7.52	−8.91	−7.51	−9.26
	B		−7.56	−8.74				
EO-01-26+0.5-2	A		−7.51	−9.65	−7.51	−9.62		
	B		−7.50	−9.59				
EO-01-25+0.5-1	A	62.5	−7.11	−10.11	−7.14	−10.07	−7.20	−10.10
	B		−7.16	−10.03				
EO-01-25+0.5-2	A		−7.03	−9.96	−7.25	−10.13		
	B		−7.48	−10.31				
EO-01-12-1	A	27.0	−5.79	−8.93	−5.72	−8.97	−5.67	−8.95
	B		−5.66	−9.01				
EO-01-12-2	A		−5.63	−8.86	−5.62	−8.92		
	B		−5.61	−8.98				
EO-01-06+1-1	A	24.9	−6.12	−10.18	−6.12	−10.09	−6.10	−10.06
	B		−6.11	−10.00				
EO-01-06+1-2	A		−6.10	−10.13	−6.08	−10.02		
	B		−6.05	−9.91				
EO-01-06+0.5-1	A	24.4	−6.21	−10.24	−6.21	−10.24	−6.20	−10.27
EO-01-06+0.5-2	A		−6.17	−10.23	−6.20	−10.31		
	B		−6.22	−10.39				
EO-01-03-1	A	16.5	−5.80	−10.18	−5.78	−10.04	−5.92	−10.06
	B		−5.76	−9.90				
EO-01-03-2	A		−6.02	−10.15	−6.05	−10.08		
	B		−6.08	−10.02				
				Bayan Ulan				
BU-02-02-01-1	A	42.5	−7.82	−9.40	−7.81	−9.35	−7.66	−9.58
	B		−7.81	−9.30				
BU-02-02-01-2	B		−7.90	−10.15	−7.90	−10.15		
BU-02-02-01-3	A		−7.31	−9.24	−7.25	−9.25		
	B		−7.19	−9.25				
BU-02-01-13-1	A	48.0	−9.23	−9.35	−9.15	−9.37	−10.54	−8.68
	B		−9.06	−9.40				
BU-02-01-13-2	A		−12.01	−8.05	−11.94	−7.99		
	B		−11.87	−7.93				
BU-02-01-12-1	A	47.5	−8.76	−7.79	−8.77	−7.61	−8.99	−8.60
	B		−8.79	−7.43				
BU-02-01-12-2	A		−8.44	−9.91	−8.68	−9.97		
	B		−8.92	−10.02				
BU-02-01-12-3	A		−9.59	−8.23	−9.53	−8.23		
	B		−9.47	−8.17				
BU-02-01-11-1	A	46.5	−8.92	−10.54	−9.01	−10.65	−8.52	−10.20
	B		−9.10	−10.75				
BU-02-01-11-2	A		−8.05	−9.68	−8.03	−9.75		
	B		−8.01	−9.82				
BU-02-01-10-1	A	46.0	−8.03	−12.56	−8.05	−12.50	−8.05	−11.58
	B		−8.06	−12.44				

TABLE 2
(Continued)

Nodule	Sample	Level (m)	Sample		Nodule		Level	
			$\delta^{13}C$	$\delta^{18}O$	$\delta^{13}C$	$\delta^{18}O$	$\delta^{13}C$	$\delta^{18}O$
BU-02-01-10-2	A		−8.17	−10.61	−8.05	−10.65		
	B		−7.92	−10.69				
BU-02-01-09-1	A	44.0	−9.15	−9.30	−9.15	−9.08	−8.70	−9.75
	B		−9.16	−8.86				
BU-02-01-09-2	A		−7.90	−11.54	−7.90	−11.34		
	B		−7.90	−11.15				
BU-02-01-09-3	A		−9.03	−8.80	−9.04	−8.82		
	B		−9.06	−8.83				
BU-02-01-08-1	A	39.5	−9.67	−7.74	−9.63	−7.75	−9.19	−8.54
	B		−9.60	−7.76				
BU-02-01-08-2	A		−8.72	−9.30	−8.75	−9.33		
	B		−8.79	−9.37				
BU-02-01-07-1	A	34.5	−9.68	−9.10	−9.73	−9.11	−9.90	−9.27
	B		−9.78	−9.13				
BU-02-01-07-2	A		−10.44	−9.04	−10.37	−9.07		
	B		−10.31	−9.10				
BU-02-01-07-3	A		−9.59	−9.62	−9.59	−9.62		
BU-02-01-07-4	A		−9.46	−7.32	−9.46	−7.32		
BU-02-01-06-1	A	33.5	−9.68	−10.18	−9.80	−10.28	−9.32	−10.41
	B		−9.91	−10.37				
BU-02-01-06-2	A		−8.78	−10.62	−8.78	−10.62		
BU-02-01-06-3	A		−9.40	−10.32	−9.40	−10.32		
BU-02-01-06-4	A		−9.66	−10.58	−9.66	−10.58		
BU-02-01-05-1	A	31.5	−8.03	−7.37	−8.06	−7.36	−8.22	−7.58
	B		−8.09	−7.35				
BU-02-01-05-2	A		−8.44	−7.82	−8.39	−7.79		
	B		−8.33	−7.76				
BU-02-01-04-1	A	25.0	−6.55	−8.47	−6.40	−8.38	−6.91	−8.38
	B		−6.25	−8.29				
BU-02-01-04-2	A		−9.50	−8.15	−9.57	−8.11		
	B		−9.64	−8.07				
BU-02-01-04-3	A		−4.80	−8.67	−4.77	−8.64		
	B		−4.73	−8.60				
BU-02-01-02-1	A	22.0	−7.95	−7.12	−7.74	−7.07	−7.93	−7.86
	B		−7.54	−7.01				
BU-02-01-02-2	A		−6.93	−8.62	−6.97	−8.65		
	B		−7.01	−8.67				
BU-02-01-02-3	A		−9.09	−7.53	−9.09	−7.53		
BU-02-01-01-1	A	15.0	−7.81	−10.20	−7.62	−10.51	−7.74	−9.14
	B		−7.43	−10.81				
BU-02-01-01-2	A		−7.50	−9.00	−7.66	−8.81		
	B		−7.82	−8.62				
BU-02-01-01-3	A		−8.04	−8.20	−7.93	−8.12		
	B		−7.82	−8.03				
BU-01-01-05-1	A	12.4	−7.32	−8.88	−7.29	−8.90	−7.18	−8.59
	B		−7.25	−8.91				
BU-01-01-05-2	A		−7.06	−8.39	−7.07	−8.29		
	B		−7.08	−8.18				
BU-01-01-04-1	A	8.0	−7.38	−8.13	−7.38	−8.47	−7.30	−8.58
	B		−7.38	−8.82				

TABLE 2
(Continued)

Nodule	Sample	Level (m)	Sample $\delta^{13}C$	Sample $\delta^{18}O$	Nodule $\delta^{13}C$	Nodule $\delta^{18}O$	Level $\delta^{13}C$	Level $\delta^{18}O$
BU-01-01-04-2	A		−7.22	−8.73	−7.22	−8.68		
	B		−7.22	−8.64				
BU-01-01-02-1	A	3.2	−6.68	−10.46	−6.77	−10.62	−6.82	−10.62
	B		−6.85	−10.78				
BU-01-01-02-2	A		−6.73	−10.57	−6.79	−10.61		
	B		−6.86	−10.66				
BU-01-01-02-3	A		−6.83	−10.64	−6.91	−10.63		
	B		−6.98	−10.63				
BU-01-01-01-1	A	1.5	−6.30	−8.61	−6.37	−8.71	−6.37	−8.71
	B		−6.43	−8.80				
				Huheboerhe				
HH-02-01-10-1	A	53.8	−7.26	−9.13	−7.26	−9.21	−9.22	−8.87
	B		−7.28	−9.25				
	C		−7.23	−9.19				
	D		−7.28	−9.26				
HH-02-01-10-2	A	−9.50	−8.17	−9.53	−8.16			
	B	−9.53	−8.03					
	C	−9.55	−8.28					
HH-02-01-10-3	A	−11.22	−7.15	−11.22	−7.15			
HH-02-01-10-4	A	−10.43	−8.67	−10.43	−8.67			
HH-02-01-10-5	A	−7.66	−11.18	−7.66	−11.18			
HH-02-01-09-1	A	49.3	−7.18	−8.53	−7.08	−8.54	−7.28	−8.88
	B		−6.99	−8.55				
HH-02-01-09-2	A		−7.50	−9.21	−7.48	−9.22		
	B		−7.46	−9.22				
HH-02-01-11U-1	A	48.3	−7.06	−8.93	−7.09	−8.97	−7.14	−9.00
	B		−7.03	−8.87				
	C		−7.35	−8.99				
	D		−6.91	−9.09				
HH-02-01-11U-2	A		−7.16	−8.92	−7.20	−9.04		
	B		−7.06	−8.94				
	C		−7.21	−9.03				
	D		−7.35	−9.26				
HH-02-01-11L-1	A	47.8	−9.99	−9.65	−10.43	−9.84	−8.13	−10.15
	B		−10.24	−9.83				
	C		−10.39	−9.93				
	D		−11.10	−9.97				
HH-02-01-11L-2	A		−6.16	−10.45	−5.82	−10.45		
	B		−5.87	−10.05				
	C		−5.42	−10.58				
HH-02-01-08-1	A	44.8	−8.65	−8.81	−8.74	−9.03	−8.75	−9.02
	B		−8.83	−9.24				
HH-02-01-08-2	A		−8.63	−9.01	−8.76	−9.02		
	B		−8.89	−9.03				
HH-02-01-07-1	A	43.3	−5.13	−9.05	−5.07	−9.13	−5.46	−9.44
	B		−5.00	−9.22				
HH-02-01-07-2	A		−5.87	−9.77	−5.86	−9.75		
	B		−5.84	−9.73				

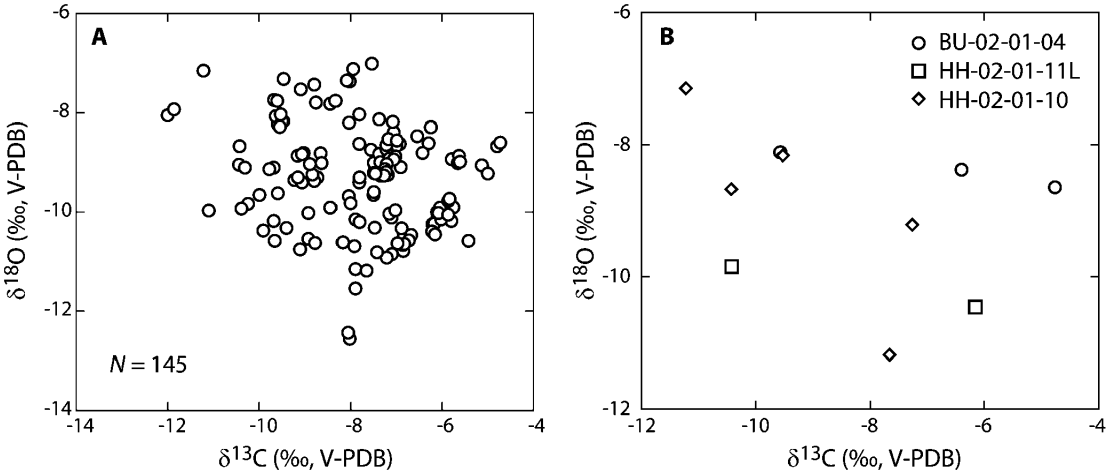

Fig. 7. Carbon and oxygen isotope compositions of paleosol carbonate. **A,** All data, with values for individual analyses shown. No pervasive pattern of covariation between $\delta^{13}C$ and $\delta^{18}O$ is apparent. **B,** Nodule average values for three sites with atypically large $\delta^{13}C$ or $\delta^{18}O$ variability. All sites exhibit positive covariation between $\delta^{13}C$ and $\delta^{18}O$. At BU-02-01-04 and HH-02-01-11L variability is much greater for $\delta^{13}C$ than for $\delta^{18}O$, whereas at HH-02-01-10 variablility for $\delta^{18}O$ exceeds that for $\delta^{13}C$. In the former case, $\delta^{13}C$ variation among carbonate nodules likely reflects spatial or temporal variation in the $\delta^{13}C$ of carbon in the soil system. In the latter, diagenesis may have altered the isotopic composition of some nodules.

of sediment deposition or early diagenesis, and are thus useful for magnetostratigraphy. Most samples carried multicomponent natural remanent magnetization, and whereas the low-temperature component isolated in most samples exhibits normal field directions, the high-temperature component displays both normal and reversed field polarities. Mean normal and reversed directions for alpha and beta sites are roughly antipodal, and pass the

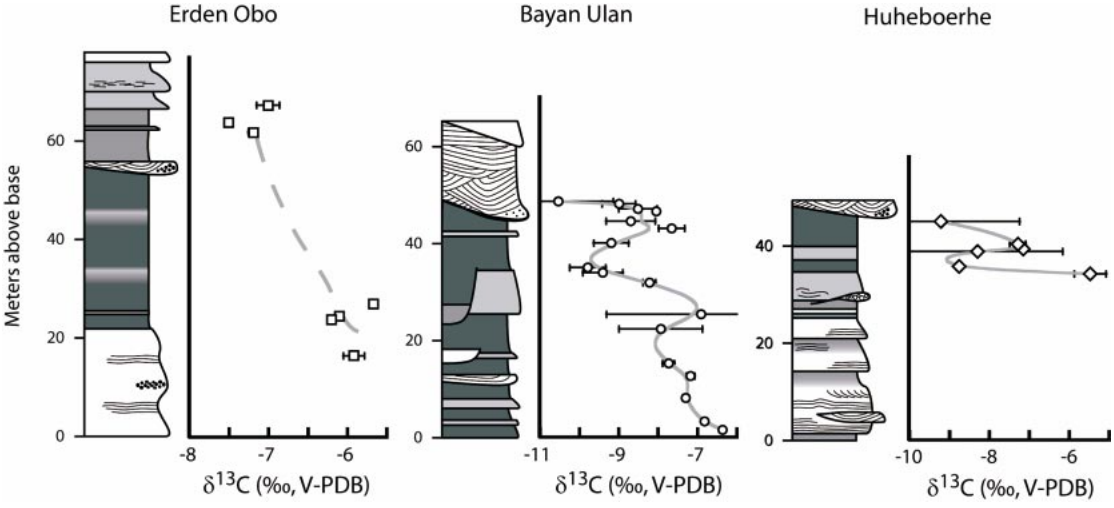

Fig. 8. Average carbon isotope values from paleosol carbonate nodules by level. Error bars are ranges for nodule average $\delta^{13}C$ at each level. All three sections preserve a similar range of values, and show a decrease in $\delta^{13}C$ through time.

reversal test of McFadden and McElhinny (1990) at 95% confidence. The somewhat different inclinations for the normal and reversed polarity averages may reflect shallowing of the reversed field directions due to the presence of a minor, secondary magnetization that was not fully removed during thermal demagnetization (e.g., Scott and Hotes, 1996). Our average normal and reversed site directions are not statistically different at 95% confidence from previously reported normal ($D = 359.6°$, $I = 53.7°$, $N = 8$, $k = 65.9$) and reversed ($D = 175.8°$, $I = -67.4°$, $N = 5$, $k = 67.1$) directions of Tertiary volcanic rocks in Inner Mongolia (Zhao et al., 1994). Again, the inclination for our reversed sites is somewhat lower than in the Zhao et al. (1994) study, suggesting the persistence of a minor magnetic overprint in these samples. Normal and reversed sample polarities are consistent among multiple samples at most sites, and site mean polarities defined coherent stratigraphic polarity intervals. In addition to these considerations, strong support for the fidelity of our paleomagnetic polarity record is provided by the consistency of magnetic, isotopic, lithologic, and biostratigraphic constraints on the correlation of the three measured sections, as discussed below.

Fidelity of the Isotopic Record

Carbon isotopes in authigenic soil carbonate reflect the $\delta^{13}C$ of soil CO_2, which below ~50 cm depth within the soil is largely derived from the decomposition of soil organic matter (e.g., Cerling, 1984). The $\delta^{13}C$ value of CO_2 respired from soil organic matter is similar to that of carbon fixed from the atmosphere by plants living on the soil (Bowen and Beerling, 2004), meaning that carbonate formed at depth within a soil provides an indirect proxy of atmospheric $\delta^{13}C$. Because atmospheric CO_2 is well mixed over the timescales on which soil carbonate form (1–100 ky; e.g., Birkeland, 1999), large changes in the $\delta^{13}C$ of the atmosphere through time should be reflected in aggrading sequences of carbonate-bearing paleosols and can be used to correlate widely separated terrestrial sedimentary sections (Koch et al., 1992; Cojan et al., 2000; Bowen et al., 2002). Diagenesis of soil carbonate isotope signatures has been observed (e.g., Budd et al., 2002), however, and the potential for diagenetic artifacts must be addressed before attempting to use our paleosol carbonate $\delta^{13}C$ record as a tool for correlation.

Careful examination of the variation and covariation of $\delta^{13}C$ and $\delta^{18}O$ values provides a useful method for identifying diagenetic overprinting in many cases (e.g., Bowen et al., 2001), although such an approach may fall short for soils formed in environments with high diagenetic potential (Budd et al., 2002). We can present two expectations for changes in isotopic signatures during diagenesis that might help identify cases where $\delta^{13}C$ values have been altered. First, diagenesis should lead to characteristic changes in intra- and internodule isotopic variability, the nature of which will depend on the degree of alteration. If alteration is partial, it should increase intranodule isotopic variability, and in some cases internodule variability, through the precipitation of diagenetic phases with different $\delta^{13}C$ and/or $\delta^{18}O$ values than the preserved, primary material. In contrast, complete alteration would produce very low intra- and internodule variability, as all values would be shifted to that of the diagenetic phase. Second, because diagenetic fluids have much more oxygen than carbon, postburial should alter $\delta^{18}O$ preferentially relative to $\delta^{13}C$.

The narrow range of within-nodule isotopic variation observed in Erlian Basin samples is similar to that seen in other studies of well-preserved paleosol carbonate micrite, but the within-level variation for many paleosols is somewhat greater (e.g., Koch et al., 1995; Bowen et al., 2001). Examination of within-level variation on a case-by-case basis shows that there is no strong relation between $\delta^{13}C$ and $\delta^{18}O$ variation within individual paleosols (fig. 9), and that many of those paleosols with the greatest internodule variability for $\delta^{13}C$ have relatively low $\delta^{18}O$ ranges (figs. 7B, 9). The one exception is site HH-02-01-10, where the very high range reported for $\delta^{18}O$ results from a single analysis of a small nodule, which gave a $\delta^{18}O$ value almost 2‰ lower than for any other sample from that level. In general, these observations are not consistent with the expectations

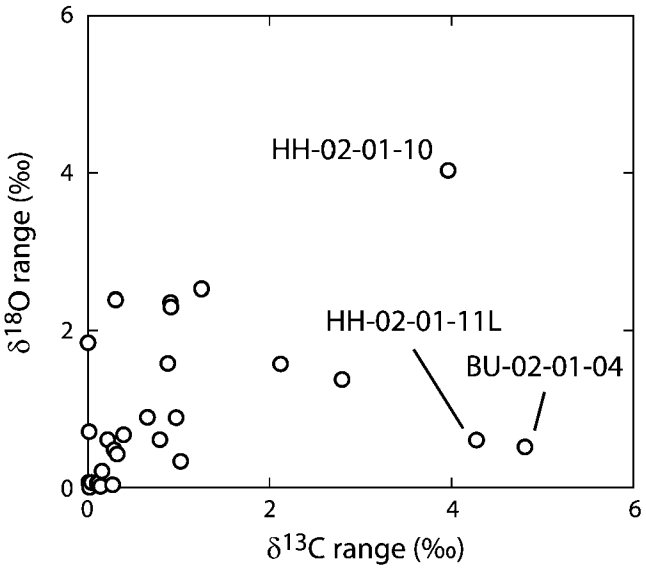

Fig. 9. Ranges of $\delta^{13}C$ and $\delta^{18}O$ values (maximum–minimum) measured for multiple carbonate nodules from individual paleosols. Labels indicate the position of high variability sites that are shown in figure 7B.

put forward for the effects of diagenetic alteration, and it seems likely that many of our samples preserve the isotopic signature of the soils in which they formed.

Although we are reasonably confident that diagenesis has not dramatically changed the $\delta^{13}C$ values of our paleosol carbonate samples, it would still be useful to understand the possible causes of atypically large $\delta^{13}C$ variation in some of the paleosols sampled. We cannot choose among alternatives with the data currently available, but we can suggest at least three possible sources of variation. First, it is possible that different nodules from these paleosols are sampling landscape-level variation in plant $\delta^{13}C$ values. The $\delta^{13}C$ of plants using the C3 photosynthetic pathway varies by ~11‰ in response to environmental differences and variation in physiological tolerance among taxa (O'Leary, 1995). If the paleosols exhibiting high internodule $\delta^{13}C$ variability represent abnormally long periods of soil formation or formed in atypically dynamic environments, they may have precipitated carbonate nodules that sampled a range of natural plant/soil $\delta^{13}C$ values. Second, the history of atmospheric $\delta^{13}C$ includes several short-lived, transient shifts (Koch et al., 1992; Jahren et al., 2001), and paleosols with high internodule variability may have formed during such an event. Only one such event is known during the early Paleogene (Koch et al., 1992); therefore, this explanation could only apply to one paleosol or stratigraphic interval of high $\delta^{13}C$ variability in each of our sections, and would imply that those levels were time-equivalent. Third, it is possible that nodules in the high-variability paleosols were formed over a range of depths in the fossil soils. Soil CO_2 near the soil surface includes a greater component of atmospheric CO_2, giving it much higher $\delta^{13}C$ than CO_2 deeper within the soil. Because paleosol horizons and boundaries between stacked paleosols could not be clearly distinguished in the poorly exposed Erlian Basin sections, it is possible that the $\delta^{13}C$ values of some of the nodules sampled in our study reflect a relatively large atmospheric contribution. In this case, only the lowest $\delta^{13}C$ values from these levels should be used for chemostratigraphy to ensure that measurements reflect vegetation-derived CO_2 consistently throughout the stratigraphic section.

Intrabasinal Correlation

Using the lithostratigraphic, magnetostratigraphic, and biostratigraphic data presented

above, we propose two alternative correlations among the three local sections studied here (fig. 10). The two alternatives differ only in how the Huheboerhe section is correlated to the Bayan Ulan and Erden Obo sections. In alternative correlation A, we place the greatest weight on our lithologic data and correlate the base of the mudstone unit at Huheboerhe to that at Erden Obo (fig. 10A). In alternative B, we correlate the Huheboerhe section to Erden Obo based on the single normal polarity site at Huheboerhe. For alternative B, the placement of the Huheboerhe section relative to the others is some ~15 m lower than for correlation A (fig. 10B). The composite stratigraphic section implied by correlation A includes five magnetic polarity zones, which we designate A+ through E+, whereas the composite section implied by alternative correlation B includes four polarity zones, here designated a−, A+, B−, and E+ (fig. 10).

Both alternative correlations presented here assume that the main (mudstone) normal polarity zones at Huheboerhe and Bayan Ulan represent continuous deposition under normal polarity conditions (e.g., no reversals are missed). Although it is possible that our sampling may not capture a reversed polarity zone occurring during the time of deposition of this rock package in one of these sections, we feel that our dense magnetostratigraphic sampling of these units and the consistency of lithostratigraphic and biostratigraphic patterns in the two sections supports the interpretation that this is a distinct polarity interval that can be correlated among the sites. Furthermore, no significant erosional surfaces were observed in the mudstone interval at Huheboerhe (with the exception of the major sandstone scour at the top of the section) or in the lower, fossiliferous part of the Bayan Ulan mudstone interval. We believe that it is unlikely that a reversed polarity interval was removed from this part of our sections as a result of erosion. A greater degree of channeling was observed in the middle part of the Bayan Ulan mudstone interval, and we cannot rule out the possibility that polarity zones may have been lost in that part of the section. Those eroded beds occur above the fossiliferous levels considered here, though, and the loss of magnetostratigraphic from that interval would not significantly affect the main conclusions of our study.

Both correlations are consistent with the majority of our stratigraphic data, and each has its own strengths and weaknesses. The main strengths of alternative correlation A are that it aligns the transition from sandstone to mudstone deposition at Erden Obo and Huheboerhe and that it pairs the relatively low (−8 to −9‰) $\delta^{13}C$ values from the upper mudstone beds at Huheboerhe with the similar $\delta^{13}C$ values in the middle of the mudstone units at the other sites. Under correlation B, these low paleosol carbonate $\delta^{13}C$ values would correlate to an interval in the other two sections where $\delta^{13}C$ values in the other sections are between 1 and 3‰ higher. In contrast, the primary shortcoming of alternative A is that it correlates the single normal polarity magnetostratigraphy site at Huheboerhe within a relatively well-sampled reversed zone at Bayan Ulan. Further magnetostratigraphic sampling will be necessary to clearly distinguish between these two alternative correlations.

Using correlation A, we propose a preliminary composite stratigraphic section for the interval of study in Erlian Basin (fig. 11). The composite section shows an up-section decline in paleosol carbonate $\delta^{13}C$, five magnetic polarity zones, and three distinct biostratigraphic intervals. Gashatan fossils occur from the base of the composite section, just below the base of polarity zone A+, to approximately the midpoint of polarity zone D−. Bumbanian fossils range from the middle of zone to the top of D−, and Irdin Manhan fossils first appear well above the base of zone E+. Paleosol carbonate $\delta^{13}C$ values decrease by ~3‰ up-section, with the highest measured values occurring near the base of polarity zone B− and the lowest within polarity zone E+. There is some suggestion that $\delta^{13}C$ values may increase slightly at the top of the section, but these data come exclusively from the poorly sampled Erden Obo section, and it is not clear that this pattern represents stratigraphic and not spatial variation. If alternative correlation B for the Huheboerhe section was adopted, the implications for the composite section would be relatively minor. In this case the poorly defined polarity zone shown as C+ in figure 11

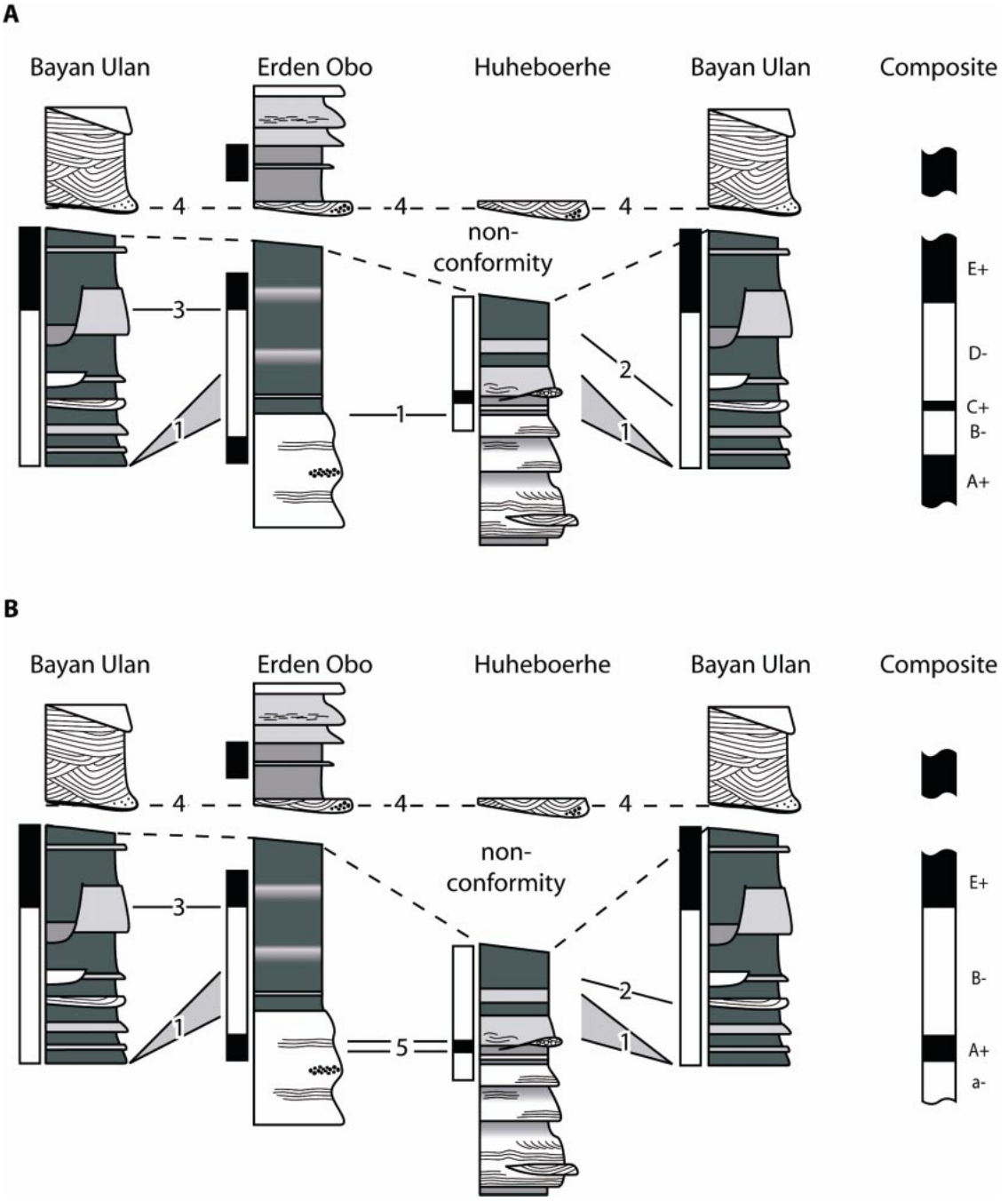

Fig. 10. Proposed correlation of measured sections and Erlian Basin composite magnetic polarity stratigraphy. **A** and **B** present two alternate hypotheses for the correlation of the Huheboerhe section. Correlation tie points in **A** and **B** include (1) base of the normal-polarity, mudrock-dominated interval; (2) base of the Bumbanian ALMA, as indicated by the first appearance of *Gomphos*; (3) normal to reversed polarity transition within the mudrock-dominated interval; and (4) erosional base of the upper sand/siltstone unit. In **B,** 5 represents correlation of the normal polarity site at Huheboerhe to the basal normal polarity zone at Erden Obo. Lithostratigraphic symbols are as in figure 2.

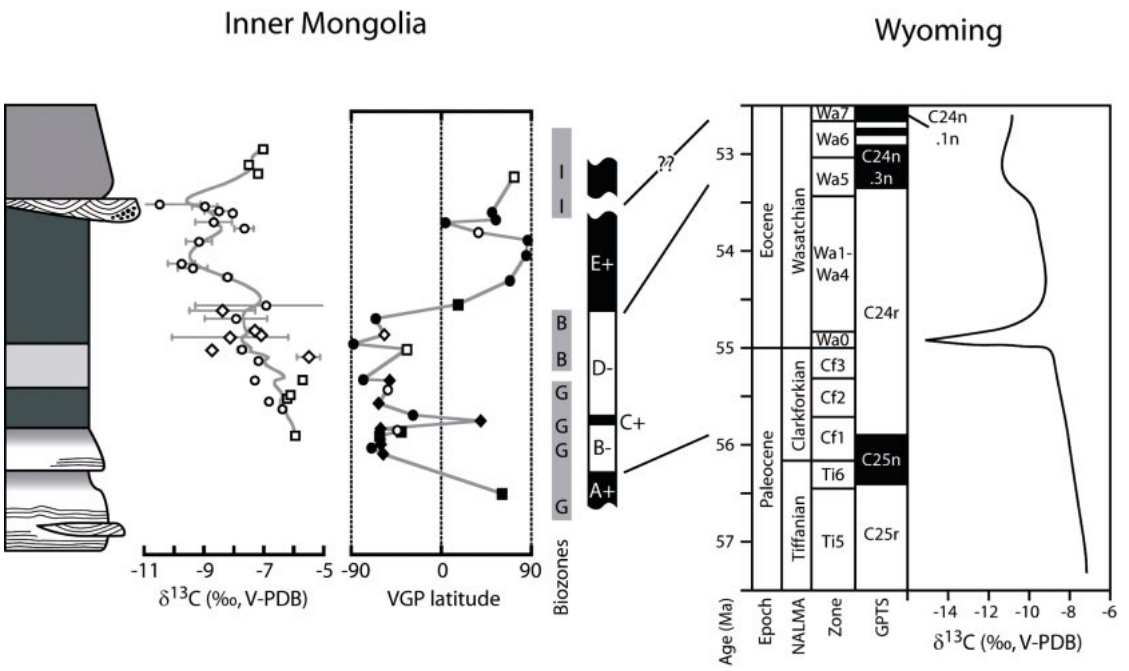

Fig. 11. Composite section and preferred correlation of Early Paleogene rocks in the Erlian Basin (left panel) to the Geomagnetic Polarity Timescale (GPTS; Cande and Kent, 1995), the sequence of North American Land Mammal Ages (NALMA), and biozones and paleosol carbonate $\delta^{13}C$ record of the Bighorn Basin, Wyoming (right panel). Data from the local sections have been combined using correlation A (fig. 10A, see text). From left to right, left panel: generalized stratigraphy, composite carbon isotope stratigraphy, composite magnetostratigraphy, stratigraphic distribution of biozones, and magnetic polarity zones for the composite section. Symbols in the isotopic and magnetic time series represent data from the Erden Obo (squares), Bayan Ulan (circles), and Huheboerhe (diamonds) local sections, and alpha and beta magnetostratigraphy sites are indicated by closed and open symbols, respectively. Biozones include the Gashatan (G), Bumbanian (B), and Irden Manha (I) ALMAs, and letters indicate the actual stratigraphic position of fossil collections. Right-hand panel is after Koch et al. (2003), with a generalized schematic carbon isotope curve based on the Bighorn Basin record shown here. Question marks indicate uncertainty in the correlation of the uppermost part of our section given that polarity zone E+ may be a composite representing more than one normal polarity chron.

would merge with zone A+ and reversed polarity zones B− and D− would be joined (see fig. 10B). The basal reversed polarity sites at Huheboerhe would then define a reversed polarity zone at the base of the composite section (a−). The Gashatan fossil *P. matyr* from Huheboerhe would be the only fossil taxon known definitively to occur within that zone, although the Gashatan assemblage from the base of the Erden Obo section is unconstrained and could correlate either within a− or the base of A+.

Age and Global Correlation

Based on the isotope, faunal, and magnetostratigraphic information summarized in our composite section (fig. 11), we propose correlations between the Erlian Basin strata and the GPTS (Cande and Kent, 1995). We can constrain the correlation of our polarity reversals to the GPTS based on the trend in paleosol carbonate $\delta^{13}C$ values in the Erlian Basin section, which we believe reflects a secular decrease in the $\delta^{13}C$ of Earth's surface carbon reservoirs from the Late Paleocene to the Early Eocene. This trend has been previously documented in marine (e.g., Zachos et al., 2001) and terrestrial carbonates (e.g., Koch et al., 1992, 2003), and is of approximately the same magnitude as that seen in our new record. The only other secular trend of comparable magnitude and the same

direction that has been documented in Early Paleogene $\delta^{13}C$ records is the rapid, transient decline in $\delta^{13}C$ at the Paleocene/Eocene boundary (Zachos et al., 2001). The entirety of the Paleocene/Eocene boundary event, however, lies within chron C24r of the GPTS, making it a poor match for the $\delta^{13}C$ shift preserved in the Erlian Basin section.

The Late Paleocene $\delta^{13}C$ high occurs within chron C26r of the GPTS, and $\delta^{13}C$ decreases steadily through time until reaching a minimum within chron C24n. In our Erlian Basin record, this decline spans polarity zones B− through E+ of the composite section (fig. 11). Previous work has confirmed that the boundary between the Gashatan and Bumbanian ALMAs occurs within the lower part of C24r (Bowen et al., 2002), and because both Gashatan and Bumbanian fossils occur in polarity zone D− we correlate this zone to C24r. We consider it to be unlikely that polarity zone C+, defined by a single normal polarity site tightly bounded by reversed sites, represents the 500-ky chron C25n, and prefer the interpretation that it represents one of the many short-lived excursions of the magnetic field (cryptochrons) which have been identified within C24r (Cande and Kent, 1995). We therefore suggest that zones B− through D− correlate to C24r and that A+ represents the top of C25n. This lowermost polarity zone is again defined by only one alpha site, but is supported by poorly clustered normal directions from two other sites at Erden Obo (not shown). The stratigraphic extent of this zone is unconstrained because it occurs at the base of the Erden Obo and Bayan Ulan sections, but it is possible that further sampling down-section at Huheboerhe could allow us to identify this polarity zone and constrain its base. Finally, we correlate the base of the uppermost polarity zone E+ to the C24r–C24n boundary. Based on the evidence for significant erosion within this part of our section and the presence of fossils thought to be of middle Eocene age (Dashzeveg and Hooker, 1997) in the upper part of E+, however, we feel that it is likely that this is a composite polarity zone including the normal subchrons within C24n and subsequent normal polarity zones.

We also present two alternative correlations which cannot be ruled out given the current data (fig. 12). Using intrabasin correlation A, we can present the alternative hypothesis that polarity zone C+ does represent chron C25n (fig. 12A). In this case, zones A+ and B− would correlate to chrons C26n and C25r, respectively. A second alternative, based on intrabasin correlation B, is identical to the preferred global correlation with the exception that the additional, basal, reversed polarity zone (designated a−) is correlated to chron C25r. Given the durations of these chrons in the GPTS, both alternatives are reasonable in that they give fairly constant sediment accumulation rates for the bounded polarity zones of the composite section. Testing these hypotheses will require further magnetostratigraphic sampling around and below the normal polarity site at Huheboerhe to identify the pattern and duration of polarity zones near and below the base of the current composite section.

The proposed correlations to the GPTS suggests that our section from the Erlian Basin represents more than 3 million years of time spanning the Paleocene/Eocene boundary. Our isotopic sampling does not appear to have recovered evidence of the 100-ky, 3–6‰ carbon isotope excursion marking the Paleocene/Eocene boundary (fig. 11). This result is not surprising given the very low sediment accumulation rates indicated for our sections by the proposed magnetostratigraphic correlations. For example, the polarity interval representing C24r according to the preferred global correlation seems to be most expanded in the Bayan Ulan section, where it is represented by at least 30 m of section. Given the estimated duration of C24r (~2.6 m.y.; Cande and Kent, 1995), this gives an average sediment accumulation rate of <1.2 cm/ky. If we assume that sedimentation was continuous, the P/E boundary event would be represented by only ~1.2 m, a thickness of rock much less than our average sampling interval. Further, there is ample evidence for significant sedimentary hiatuses and erosional down-cutting in all three of our local sections, making it even more likely that the P/E boundary $\delta^{13}C$ excursion interval was not present or not sampled in our sections.

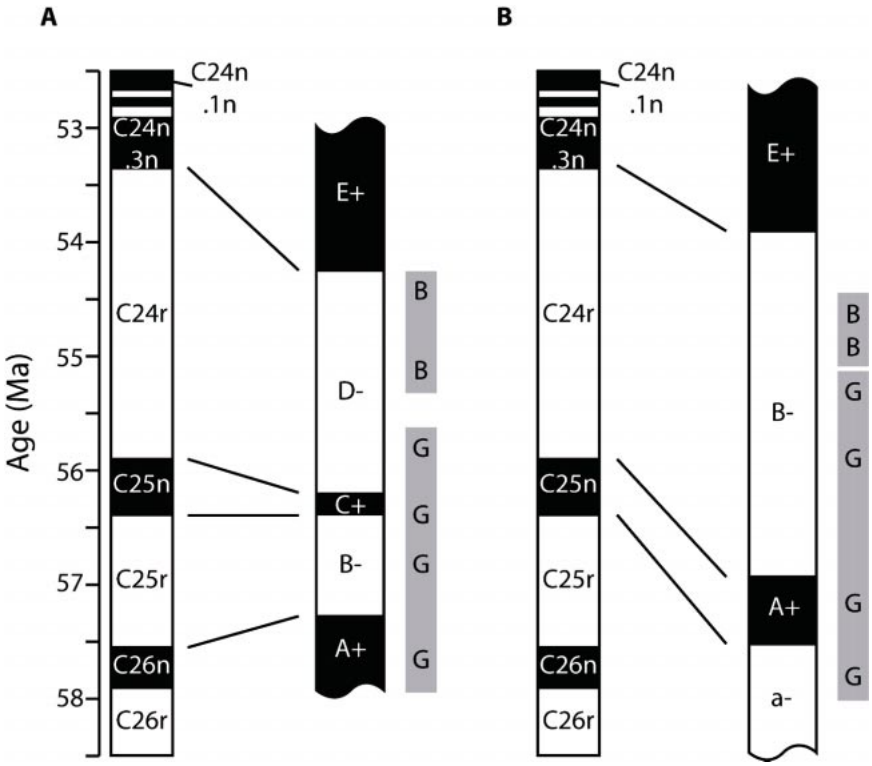

Fig. 12. Two alternative correlations of the Erlian Basin composite magnetic polarity zones and faunal zones (letter designations as in fig. 11) to the Geomagnetic Polarity Timescale. **A,** Alternative global correlation based on intrabasin correlation A (see fig. 10A). Polarity zone C+, defined by the single normal polarity site at Huheboerhe, is considered to represent chron C25n, and polarity zones A+ and B− are shifted to correspond to C26n and C25r, respectively. Only one Gashatan collection, the upper Gashatan level at Bayan Ulan containing *Palaeostylops*, *Pseudictops*, and *Palaeomylus*, falls within C24r, and the range of Gashatan faunas is extended downward into C26n. **B,** Alternative global correlation based on intrabasin correlation B (see fig. 10B). This is identical to the preferred global correlation (fig. 11) with the exception that the lower reversed polarity sites in the Huheboerhe section constitute a basal reversed polarity zone (designated a−), which is correlated to chron C25r. The range of Gashatan faunas in the composite section is extended downward into this zone by the *Prodinoceras*-bearing locality at Huheboerhe.

CONCLUSIONS: THE AGE OF EARLY PALEOGENE ALMAS

The new data from the Erlian Basin place additional constraints on the age of Early Paleogene ALMAs and their correlation to the land mammal ages of North America and Europe. These data are preliminary, and further sampling will help to resolve the exact chronostratigraphic placement of the Erlian Basin faunas, but our current findings provide evidence that faunas typical of the Gashatan ALMA persist into chron C24r. Previously, the ~900-ky interval of time between the base of C24r and the Paleocene/Eocene boundary represented an interval within which the nature of Asian faunas was unconstrained (Bowen et al., 2002; Ting et al., 2003). This window of time represented the potential extent to which Bumbanian faunas, and the Asian first appearances of ''new'' groups of mammals therein, might have predated these key first appearances on the other Holarctic continents. If modern mammals evolved and diversified in an Asian Eden before dispersing throughout the Northern Hemisphere, they did so within this interval. Under all three possible correlations of the Erlian Basin composite section to the

GPTS, Gashatan fossils are shown to range into the base of C24r, although the extent of their persistence within this chron varies substantially among correlations. According to the preferred global correlation and the alternative based on intrabasin correlation B, Gashatan faunas are found throughout more than half of the interval of the Erlian Basin composite section representing chron C24r, implying that the Gashatan ALMA must extend quite near to the Paleocene/Eocene boundary. If the alternative global correlation shown in figure 12A proves correct, however, only a single Gashatan level would lie within C24r, and significant uncertainty would remain regarding the placement of the Gashatan/Bumbanian boundary relative to the Paleocene/Eocene boundary.

Though they have received less scrutiny than the Gashatan/Bumbanian boundary, the ages of most other ALMA boundaries are almost entirely unconstrained by independent data. If either alternative correlation shown in figure 12 proves correct, the known range of Gashatan faunas will be extended downward into chron C25r and possibly C26n. This would imply that Gashatan faunas span an interval of time including the boundary between the Tiffanian and Clarkforkian NALMAs, which occurs within C25n, and that the boundary between the Gashatan and the earlier Nonshanian ALMA correlates within the Tiffanian NALMA. At this point, it is difficult to say anything concrete about the upper boundary age of the Bumbanian ALMA based on our new data. Under intrabasin correlation A, the *Gomphos* level at Huheboerhe is likely somewhat younger than that at Bayan Ulan. Although the correlation of this level relative to the C24r/C24n boundary preserved in the other two local sections is not well constrained, it appears that the Bumbanian level at Huheboerhe may lie within the upper part of C24r, making it somewhat younger than other Bumbanian faunas (Bowen et al., 2002; Ting et al., 2003). As noted above, Irdin Manhan fossils occur within what is likely to be a composite polarity interval, and further up-section sampling will be required in order to constrain their age and correlation.

The full nature and magnitude of global change occurring at the Paleocene/Eocene boundary is only now being realized. Close ties between climatic events at the P/E boundary and modernization of mammal faunas in North America and Europe have been established, but the nature of Asian faunal modernization near the P/E boundary has remained a topic of debate. By constraining the timing of taxonomic turnover for this region, we can begin to understand whether the evolutionary modernization of faunas on the Asian continent operated at its own pace, tied to the rest of the Holarctic only by episodic pulses of opportunistic interchange, or if these communities developed in pace with, and presumably in response to the same extrinsic or intrinsic forcing as, other Northern Hemisphere faunas. Our preliminary results presented here suggest that modernization of Asian faunas near the P/E boundary may have been nearly synchronous with turnover in Europe and North America, and that mammals on these three continents may have evolved in close step through this climatically and environmentally dynamic interval.

ACKNOWLEDGMENTS

We thank W. Clyde, R. Coe, G. Dickens, Thierry Smith, and Paul White for helpful reviews of this manuscript, and R. Coe, C. Pluhar, and X. Zhao of the University of California Paleomagnetics laboratory for their assistance. Funding for this work was provided by a U.S. National Science Foundation grant to Koch, Meng, and collaborators (EAR-0120727), National Natural Science Foundation of China grants to Meng (G200007707 and 49928202), and by the Institute of Vertebrate Paleontology and Paleoanthropology (IVPP) of the Chinese Academy of Sciences. Bowen was supported by a National Science Foundation Graduate Research Fellowship during part of the project. Field work in Inner Mongolia would not have been possible without the logistical and intellectual support of the staff and faculty of the IVPP.

REFERENCES

Averianov, A. 1996. Early Eocene Rodentia of Kyrgyzstan. Bulletin du Muséum National d'Histoire Naturelle, 18: 629–662.

Bao, H., P.L. Koch, and R.P. Hepple. 1998. He-

matite and calcite coatings on fossil vertebrates. Journal of Sedimentary Research 68: 727–738.

Beard, K.C. 1998. East of Eden; Asia as an important center of taxonomic origination in mammalian evolution. *In* K.C. Beard and M.R. Dawson (editors), Dawn of the age of mammals in Asia, Bulletin of the Carnegie Museum of Natural History 34: 5–39.

Beard, K.C., and M.R. Dawson. 1999. Intercontinental dispersal of Holarctic land mammals near the Paleocene/Eocene boundary; paleogeographic, paleoclimatic and biostratigraphic implications. Bulletin de la Société Géologique de France 170: 697–706.

Birkeland, P.W. 1999. Soils and geomorphology. New York: Oxford University Press, 430 pp.

Bowen, G.J., and D.J. Beerling. 2004. An integrated model for soil organic carbon and CO2: implications for paleosol carbonate pCO2 paleobarometry. Global Biogeochemical Cycles: 18, GB1026, doi:10.1029/2003GB002117.

Bowen, G.J., W.C. Clyde, P.L. Koch, S. Ting, J. Alroy, T. Tsubamoto, Y. Wang, and Y. Wang. 2002. Mammalian dispersal at the Paleocene/Eocene boundary. Science 295: 2062–2065.

Bowen, G.J., P.L. Koch, P.D. Gingerich, R.D. Norris, S. Bains, and R.M. Corfield. 2001. Refined isotope stratigraphy across the continental Paleocene-Eocene boundary on Polecat Bench in the Northern Bighorn Basin. *In* P.D. Gingerich (editor), Paleocene-Eocene stratigraphy and biotic change in the Bighorn and Clarks Fork Basins, Wyoming. University of Michigan Museum of Paleontology 33: 73–88.

Budd, D.A., S.M. Pack, and M.L. Fogel. 2002. The destruction of paleoclimatic isotopic signals in Pleistocene carbonate soil nodules of Western Australia. Palaeogeography Palaeoclimatology Palaeoecology 188: 249–273.

Cande, S.C., and D.V. Kent. 1995. Revised calibration of the geomagnetic polarity timescale for the Late Cretaceous and Cenozoic. Journal of Geophysical Research-Solid Earth 100: 6093–6095.

Cerling, T.E. 1984. The stable isotopic composition of modern soil carbonate and its relationship to climate. Earth and Planetary Science Letters 71: 229–240.

Cojan, I., M.G. Moreau, and L.E. Stott. 2000. Stable carbon isotope stratigraphy of the Paleogene pedogenic series of southern France as a basis for continental-marine correlation. Geology 28: 259–262.

Dashzeveg, D. 1988. Holarctic correlation of nonmarine Palaeocene-Eocene boundary strata using mammals. Journal of the Geological Society [London] 145: 473–478.

Dashzeveg, D. 1990. The earliest rodents (Rodentia, Ctenodactyloidea) of Central Asia. Acta Zoologica Cracoviensia 33: 11–35.

Dashzeveg, D., and J.J. Hooker. 1997. New Ceratomorph Perissodactyls (Mammalia) from the Middle and Late Eocene of Mongolia—Their implications for phylogeny and dating. Zoological Journal of the Linnean Society 120: 105–138.

Farley, K.A., and S.F. Eltgroth. 2003. An alternative age model for the Paleocene-Eocene thermal maximum using extraterrestrial He-3. Earth and Planetary Science Letters 208: 135–148.

Gingerich, P.D. 1989. New earliest Wasatchian mammalian fauna from the Eocene of northwestern Wyoming: composition and diversity in a rarely sampled high-floodplain assemblage. University of Michigan Papers on Paleontology 28: 1–97.

Gingerich, P.D. 2001. Biostratigraphy of the continental Paleocene-Eocene boundary interval on Polecat Bench in the Northern Bighorn Basin. *In* P.D. Gingerich (editor), Paleocene-Eocene stratigraphy and biotic change in the Bighorn and Clarks Fork Basins, Wyoming. University of Michigan Papers on Paleontology 33: 37–71.

Harrington, G.J. 2003. Geographic patterns in the floral response to Paleocene-Eocene warming. *In* S.L. Wing, P.D. Gingerich, B. Schmitz, and E. Thomas (editors), Causes and consequences of globally warm climates in the Early Paleogene. Geological Society of America Special Paper 369: 381–393.

Hooker, J.J. 1998. Mammalian faunal change across the Paleocene-Eocene transition in Europe. *In* M.-P. Aubry, S. Lucas, and W.A. Berggren (editors), Late Paleocene-Early Eocene climatic and biotic events in the marine and terrestrial records: 428–450. New York: Columbia University Press.

Jahren, A.H., N.C. Arens, G. Sarmiento, J. Guerrero, and R. Amundson. 2001. Terrestrial record of methane hydrate dissociation in the Early Cretaceous. Geology 29: 159–162.

Kennett, J.P., and L.D. Stott. 1991. Abrupt deep-sea warming, palaeoceanographic changes and benthic extinctions at the end of the Palaeocene. Nature 353: 225–229.

Koch, P.L., W.C. Clyde, R.P. Hepple, M.L. Fogel, S.L. Wing, and J.C. Zachos. 2003. Carbon and oxygen isotope records from paleosols spanning the Paleocene-Eocene boundary, Bighorn Basin, Wyoming. *In* S.L. Wing, P.D. Gingerich, B. Schmitz, and E. Thomas (editors), Causes and consequences of globally warm climates in the early Paleocene. Geological Society of America Special Paper 369: 49–64.

Koch, P.L., J.C. Zachos, and D.L. Dettman. 1995. Stable isotope stratigraphy and paleoclimatology of the Paleogene Bighorn Basin (Wyoming, USA). Palaeogeography Palaeoclimatology Palaeoecology 115: 61–89.

Koch, P.L., J.C. Zachos, and P.D. Gingerich. 1992. Correlation between isotope records in marine and continental carbon reservoirs near the Palaeocene/Eocene boundary. Nature 358: 319–322.

Magioncalda, R., C. Dupuis, T. Smith, E. Steurbaut, and P.D. Gingerich. 2004. Paleocene-Eocene carbon isotope excursion in organic carbon and pedogenic carbonate: direct comparison in a continental stratigraphic section. Geology 32: 553–556.

McFadden, P.L., and M.W. McElhinny. 1990. Classification of the reversal test in paleomagnetism. Geophysics Journal International 103: 725–729.

McKenna, M.C. 1973. Sweepstakes, filters, corridors, Noah's Arks, and beached Viking funeral ships in palaeogeography. *In* D.H. Tarling and S.K. Runcorn (editors), Implications of Continental Drift to the earth sciences, Vol. 1: 295–308. London: Academic Press.

Meng, J., G.J. Bowen, J. Ye, P.L. Koch, S. Ting, Q. Li, and X. Jin. 2004. Gomphos elkema (Glires, Mammalia) from the Erlian Basin: evidence for the Early Tertiary Bumbanian land mammal age in Nei-Mongol, China. American Museum Novitates 3425: 1–25.

Meng, J., A.R. Wyss, Y. Hu, J. Ye, G.J. Bowen, and P.L. Koch. In review. Glires (Mammalia) from the Late Paleocene Bayan Ulan of Inner Mongolia. American Museum Novitates.

Meng, J., R. Zhai, and A.R. Wyss. 1998. The late Paleocene Bayan Ulan fauna of Inner Mongolia, China. *In* K.C. Beard and M.R. Dawson (editors), Dawn of the age of mammals in Asia. Bulletin of the Carnegie Museum of National History 34: 148–185.

O'Leary, M.H. 1995. Environmental effects on carbon isotope fractionation in terrestrial plants. *In* E. Wada, T. Yoneyama, M. Minigawa, T. Ando, and B.D. Fry (editors), Stable isotopes in the biosphere: 78–91. Kyoto, Japan: Kyoto University Press.

Ouda, K. 2003. The Paleocene/Eocene boundary in Egypt: an overview. Micropaleontology 49: 15–40.

Rohl, U., T.J. Bralower, R.D. Norris, and G. Wefer. 2000. New chronology for the late Paleocene thermal maximum and its environmental implications. Geology 28: 927–930.

Scott, G.R., and S.A. Hotes. 1996. The reversal test—an examination of secondary directions. Geophysical Research Letters 23: 1805–1808.

Shevyreva, N.S. 1989. New rodents (Ctenodactyloidea, Rodentia, Mammalia) from the Lower Eocene of Mongolia. Paleontologicheskyi Zhurnal 3: 60–72. [in Russian]

Smith, T. 2000. Mammals from the Paleocene-Eocene transition in Belgium (Tienen Formation, MP7): paleobiogeographical and biostratigraphical implications. GFF (Geologiska Foreningens i Stockholm Forhandlingar) 122: 148–149.

Smith, T., J. Van Itterbeeck, and P. Missiaen. 2004. Oldest Plesiadapiform (Mammalia, Proprimates) from Asia and its paleobiogeographic implicatoins for faunal interchange with North America. Comptes Rendus de l' Académie des Sciences, Paris 3: 43–52.

Steurbaut, E., J. De Coninck, E. Roche, and T. Smith. 1999. The Dormaal Sands and the Paleocene/Eocene boundary in Belgium. Bulletin de la Société Géologique de France 170: 217–227.

Ting, S. 1998. Paleocene and early Eocene land mammal ages of Asia. *In* K.C. Beard and M.R. Dawson (editors), Dawn of the age of mammals in Asia, Bulletin of the Carnegie Museum of National History 34: 124–147.

Ting, S., G.J. Bowen, P.L. Koch, W.C. Clyde, Y. Wang, and M.C. McKenna. 2003. Biostratigraphic, chemostratigraphic, and magnetostratigraphic study across the Paleocene/Eocene boundary in the Hengyang Basin, Hunan, China. *In* S.L. Wing, P.D. Gingerich, B. Schmitz, and E. Thomas (editors), Causes and consequences of globally warm climates in the Early Paleogene. Geological Society of America Special Paper 369: 521–535.

Tong, Y., and J. Wang. 1998. A preliminary report on the early Eocene mammals of the Wutu fauna, Shandong Province, China. *In* K.C. Beard and M.R. Dawson (editors), Dawn of the age of mammals in Asia, Bulletin of the Carnegie Museum of National History 34: 186–193.

U. S. Geological Survey. 1996. GTOPO30 global 30 arc second elevation data. Sioux Falls, SD: USGS EROS Data Center.

Watson, G.S. 1956. A test for randomness of directions. Monthly Notices of the Royal Astronomical Society Geophysical Supplement 7: 160–161.

Wing, S.L., H. Bao, and P.L. Koch. 1999. An early Eocene cool period? Evidence for continental cooling during the warmest part of the Cenozoic. *In* B.T. Huber, K.G. Macleod, and S.L. Wing (editors), Warm climates in Earth history: 197–237. Cambridge: Cambridge University Press.

Zachos, J.C., K.C. Lohmann, J.C.G. Walker, and S.W. Wise. 1993. Abrupt climate changes and

transient climates during the Paleogene; a marine perspective. Journal of Geology 101: 191–213.

Zachos, J.C., M. Pagani, L. Sloan, E. Thomas, and K. Billups. 2001. Trends, rhythms, and aberrations in global climate 65 Ma to present. Science 292: 686–693.

Zhao, X., R.S. Coe, Y. Zhou, S. Hu, H. Wu, G. Kuang, Z. Dong, and J. Wang. 1994. Tertiary paleomagnetixm of North and South China and a reappraisal of late Mesozoic paleomagnetic data from Eurasia: implications for the Cenozoic tectonic history of Asia. Tectonophysics 235: 181–203.

Complete lists of all issues of the *Novitates* and the *Bulletin* are available at World Wide Web site http://library.amnh.org/pubs. Inquire about ordering printed copies via e-mail from scipubs@amnh.org or via standard mail from: American Museum of Natural History, Library—Scientific Publications, Central Park West at 79th St., New York, NY 10024. TEL: (212) 769-5545. FAX: (212) 769-5009.

♾ This paper meets the requirements of ANSI/NISO Z39.48-1992 (Permanence of Paper).